J Mater Sci (2010) 45:5820–5830
DOI 10.1007/s10853-010-4658-2

Orthotropic properties of loblolly pine (*Pinus taeda*) strands

Gi Young Jeong · Daniel P. Hindman · Audrey Zink-Sharp

Received: 23 February 2010 / Accepted: 25 May 2010 / Published online: 12 June 2010

Abstract Orthotropic properties of loblolly pine strands were measured from growth ring numbers 1–10 and 11–20 using digital image correlation (DIC). Eight elastic properties (E_L, E_R, E_T, G_{LR}, G_{LT}, υ_{LR}, υ_{LT}, and υ_{RT}) and five strength values (σ_L, σ_R, σ_T, τ_{LR}, and τ_{LT}) of loblolly pine strands were measured. Compliance matrices were derived and used to calculate the maximum normal and shear strains. With the increment of growth ring number, elastic modulus and ultimate tensile strength (UTS) generally increased, whereas shear strength decreased. Statistical comparison showed that elastic moduli, Poisson's ratio, and UTS were highly dependent upon orientation of strands with loading direction. Only elastic modulus and UTS from the longitudinal-radial plane strands were significantly different by the two growth ring positions. More distinctive orthotropic properties of loblolly pine strands from growth ring numbers 11–20 were found associated with more consistent failure modes.

G. Y. Jeong (✉)
Sustainable Engineered Material Institute, Virginia Polytechnic Institute and State University, 230 Cheatham Hall, Blacksburg, VA 24061-0323, USA
e-mail: gjeong1@vt.edu

D. P. Hindman
Department of Wood Science and Forest Products, Virginia Polytechnic Institute and State University, Brooks Forest Products Center, 1650 Ramble Road, Blacksburg, VA 24061-0503, USA

A. Zink-Sharp
Department of Wood Science and Forest Products, Virginia Polytechnic Institute and State University, 230 Cheatham Hall, Blacksburg, VA 24061-0323, USA

Introduction

Comprehensive studies of orthotropic properties of different wood species were done by [1–3]. These researchers used plate bending tests to evaluate the elastic properties of different wood species. However, it is doubtful whether orthotropic properties of wood evaluated from plate test could apply to the wood strands.

When wood strands are processed with a flaker, surface damage can be created, which could result in a lower elastic modulus and strength compared to structure size lumber [4–6]. Earlywood and latewood mechanical properties have been found to be significantly different throughout different growth ring numbers [7–9]. As wood material is located further away from the pith, characteristics of cellular structures change from juvenile to mature wood. Compared to mature wood, juvenile wood contains higher microfibril angles, a greater percentage of compression wood, distorted grain patterns, and a lower percentage of latewood [10].

Structural differences and processing may cause differences in orthotropic properties of wood strands compared to the orthotropic properties of wood evaluated from the previous studies. The fundamental study has not been completed for measuring material properties of wood strands as a main component of the engineered wood products. If engineered wood products can be designed based on known material properties of the wood strands, specific targeted properties could be achieved with minimal time and resources [11–13].

Literature review

Previous studies used different test methods to evaluate the elastic modulus and ultimate tensile strength (UTS) of

wood strands from different species [4–6, 14–17]. Comprehensive results from previous research can be found in Jeong et al. [6].

Jeong et al. [6] noted that previous research on measurement of mechanical properties from wood strands cannot be directly comparable due to different testing arrangements. To investigate the effect of the testing arrangement on mechanical properties of loblolly pine (*P. taeda*) strands, different loading rates and different thicknesses of wood strands were used. While there was no significant difference of elastic modulus and UTS over the range of loading rates, there was a significant difference of elastic modulus and UTS from different thicknesses. As strand thickness increased, elastic modulus and UTS increased. Testing arrangements for wood strands including loading rate and thickness of wood strands were suggested.

Zhang and Sliker [18] measured the in-plane shear modulus from different species—redwood (*Sequoia sempervirens*), sugar pine (*Pinus lambertiana*), white pine (*Pinus strobus*), basswood (*Tilia americana*), cottonwood (*Populus deltoides*), white ash (*Fraxinus americana*), and yellow-poplar (*Liriodendron tulipifera*) using off-axis tension and compression tests. Shear measurements from off-axis tension tests showed less distortion by the crosshead compared to off-axis compression tests. From the off-axis tension and compression tests, grain angles of 14–35° were recommended to measure the shear modulus of wood.

Jeong et al. [9] evaluated mechanical properties of earlywood and latewood of loblolly pine from growth ring numbers 1–10 and 11–20 using digital image correlation (DIC). As growth ring number increased, elastic modulus, UTS, and Poisson's ratio from earlywood and latewood increased, except for specific gravity and UTS from latewood. While elastic modulus values from earlywood and latewood were not dependent upon specific gravity, the UTS values were highly related with specific gravity. Earlywood and latewood showed different strain distribution related to their structures.

Galicki and Czech [19] measured UTS of four different orientations (0, 30, 45, and 90°) from Scots pine (*Pinus silvestris*). The UTS from orientation angles up to 25° was dependent upon density, and the specimens showed a transverse rupture in the latewood and earlywood band. However, the UTS of 30, 45, and 90° orientation strands was not related with density, and specimens showed failure only within the earlywood band.

In processing wood strands, understanding the effects of the orientation and growth ring numbers on the mechanical properties is crucial to maximize the end-use properties. Segregation of different strands into discrete categories can maximize the benefits of use. The aim of this study was to complete orthotropic properties of loblolly pine strands from growth ring numbers 1–10 and 11–20 using DIC. Orthotropic constitutive matrices were complete, and the orthotropic failure behaviors under tension loading were presented.

Materials and methods

Specimen preparation

A 25-year-old loblolly pine (*Pinus taeda*) from Reynolds Homestead Research Center in Patrick County, Virginia was chosen for this study. A wood disk was cut approximately 0.6 m height from the ground. Figure 1 shows a loblolly pine disk and the different planes of a loblolly pine block, and the final wood strand orientation with dimensions. Owing to the manner of tree growth and arrangement of wood cells within the stem, three orthogonal axes can be defined for wood. These three axes are used to construct the longitudinal (L), the radial (R), and the tangential (T) axes. The longitudinal direction is parallel to the direction of the fibers (tracheids) and has the highest elastic stiffness and strength. The radial and tangential directions are perpendicular to the direction of the fibers. The radial direction is parallel to the rays and perpendicular to the growth rings. The tangential direction is perpendicular to the rays and tangential to the growth rings. As it can be seen from Fig. 1, there is no true tangential direction. The tangential direction exists after the longitudinal and radial directions are defined. Wood is somewhat stronger and stiffer in the radial direction compared to the tangential direction. These strength differences are related to the cellular structure of wood [20].

Wood blocks of size 146 mm by 146 mm by 25.4 mm from growth ring numbers 1–10 and 11–20 were prepared from a loblolly pine disk to generate wood strands. Wood

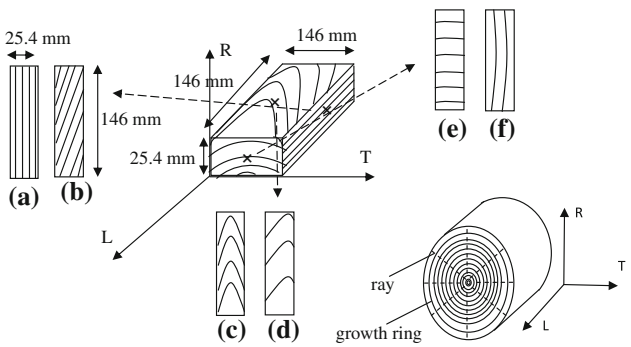

Fig. 1 Six differently oriented strands used in testing. **a** longitudinal-radial plane strands, **b** longitudinal-radial angled plane strands, **c** longitudinal-tangential plane strands, **d** longitudinal-tangential angled plane strands, **e** radial-tangential plane strands, and **f** tangential-radial plane strands

Table 1 Nomenclature and sample size for different orientations of wood strands from different growth ring numbers

Nomenclature	Plane	Growth ring number	Number of samples
LR 1-10	Longitudinal-radial	1–10	30
LR 11-20	Longitudinal-radial	11–20	30
LT 1-10	Longitudinal-tangential	1–10	30
LT 11-20	Longitudinal-tangential	11–20	30
LRA 1-10	Longitudinal-radial angled	1–10	30
LRA 11-20	Longitudinal-radial angled	11–20	30
LTA 11-20	Longitudinal-tangential angled	11–20	30
TR 11-20	Tangential-radial	11–20	30
RT 1-10	Radial-tangential	1–10	30
RT 11-20	Radial-tangential	11–20	30

blocks were sliced using a band saw. After all wood blocks were marked for growth ring number, the blocks were soaked in water and placed under a vacuum overnight to minimize surface damage during flaking. Strands were processed with a flaker located at the Brooks Forest Products Center at Virginia Polytechnic Institute and State University. As a result of the method of strand generation and the availability of material, finer gradations into discrete growth rings were not obtained, but strands from growth ring numbers 1–10 and 11–20 were obtained to investigate the effect of growth ring positions on orthotropic properties of loblolly pine strands.

From the two different growth ring positions, six representative orientation strands of size 146 mm by 25.4 mm by 0.762 mm were cut from each plane, (a) longitudinal-radial, (b) longitudinal-radial angled, (c) longitudinal-tangential, (d) longitudinal-tangential angled, (e) radial-tangential, and (f) tangential-radial planes. The longitudinal-radial plane was formed by L and R axes that were exposed when the cut was done along the longitudinal axis of the stem and perpendicular to the growth rings. The wide surface of the strand was the radial direction. The longitudinal-tangential plane was the exposed plane of L, T axes. The wide surface of the strand was approximately tangent to the growth rings. For best results in evaluation of shear modulus [18], longitudinal-radial angled and longitudinal-tangential angled plane strands were cut to 30° (θ) from the longitudinal direction. The tangential-radial plane and radial-tangential plane were formed by T and R axes that were exposed when wood was cut at right angles to the longitudinal axis of the stem. The wide surface for the tangential-radial plane strand was the radial direction. The wide surface for the radial-tangential plane strand was approximately tangent to the growth rings. Strands from growth ring numbers 1–10 on the longitudinal-tangential angled and tangential-radial plane could not be prepared due to the lack of dimension and brittleness of the material in those planes. All strands were conditioned to stabilize at 6% equilibrium moisture content in the environment chamber for 1 month before testing. Table 1 shows nomenclature and sample sizes for each growth ring number and plane.

Test methods

Tension tests used an MTS universal testing machine and DIC to determine elastic modulus, shear modulus, Poisson's ratio, UTS, and shear strength of wood strands. The elastic modulus and Poisson's ratio from differently oriented strands were obtained by synchronizing loading data from the MTS testing machine with elastic strain values from a DIC technique, whereas UTS and shear strength were obtained using the peak load values. Figure 2 illustrates the testing setup. The MTS universal testing machine was equipped with a 889N load cell. Loading rate was 0.025 cm/min. and distance between the grips was 10.16 cm. Different loading increments (4.4 N, 22.2 N, 44.4 N, and 66.7 N) and loading speeds (0.00254 cm/min, 0.0254 cm/min, and 0.254 cm/min) were used to determine the testing conditions for measuring the elastic properties of differently oriented strands by comparing with the MOE

Fig. 2 Experimental tensile test setup for digital image correlation

values determined using an extensometer. Preliminary testing found that a 44.4 N loading increment for the LR and LT plane strands, a 22.2 N loading increment for the LRA and LTA plane strands, and a 4.4 N loading increment for the TR and RT plane strands at loading rate of 0.0254 cm/min were best for the elastic property measurements of strands.

For the LR, LT, LRA, and LTA plane strands, a 22.2 N preload was applied to prevent slippage of the grip, and for the TR and RT plane strands, a 4.44 N preload was applied to prevent slippage of the grip. Incremental loading was applied to prevent the capture of distorted images. Capture of images during continuous loading can cause strain greater than true strain [21]. To determine the influence of short incremental pauses, a test was conducted in which loading was paused for 1 min while each image was captured. The results of this testing showed only 1% strain change. Therefore, any influence of a pause on the strain variation can be considered negligible.

A sequence of images was captured during the test using a CCD camera (Model PL-A662) from Pixel Link Megapixel Firewire Camera. The CCD camera was mounted on a stand with a macro adjustable holder. An Optem Zoom 70 lens with magnification of 0.75× was attached to the camera, and a fiber optic light was used to illuminate the test specimen surface. The distance between lens and object was adjusted to produce a clear image. The camera was placed on a desk separate from the MTS testing machine, and rubber pads were put under the camera stand to prevent vibration when the images were taken. To minimize the influence of light other than from the fiber optic lamp, all testing was conducted at night with no direct room light.

Pixel size of the image was 1280 by 1024 pixels with an 8-bit gray level. The pixel size was converted to spatial size for the determination of displacement. Horizontal and vertical lengths of the image taken were 10 mm by 8 mm. Spatial size of the pixel was calculated to be 9.76 μm/pixel by 6.25 μm/pixel.

Baxter and Graham [22] and Baxter et al. [23] proposed a moving window generalized method of cells (MW-GMC) to characterize material properties of composite materials based on digitized images of local microstructure of the material. The statistical variability of material properties of composite material was dependent upon the window size. Larger window sizes produced smaller variance of material properties. However, if window size becomes too large, the variability of material properties approaches zero. A smaller window size produces noisier fields, and requires higher computational effort. The choice of window size in this study was emphasized to represent the local material properties. Different window sizes, 200, 100, 50, 25, 15, and 10 pixel, were used to check the convergence of strain

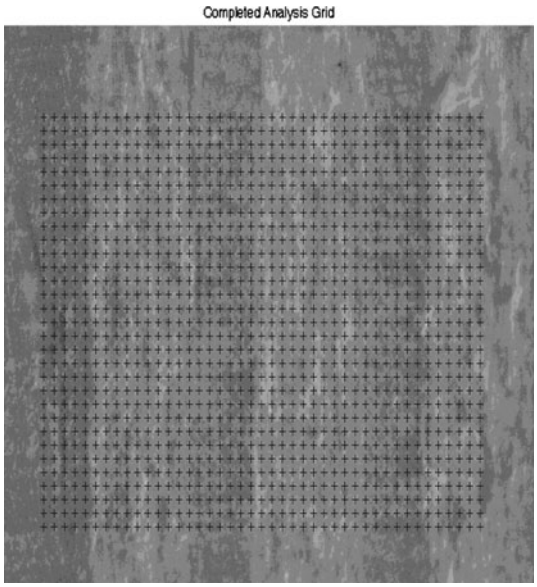

Fig. 3 A virtual grid generated on the digital image of a strand

value. A 25 by 25 pixel size (0.244 mm by 0.156 mm) of window was chosen to represent the local material properties of strands. The window was generated on the digital image of the surface of the wood strands. The position of the window was recorded as x, y coordinate of the pixel position on the image. Figure 3 describes the window generated on the reference digital image of a strand.

Elastic modulus (E), Poisson's ratio, and UTS of differently oriented strands from growth ring numbers 1–10 and 11–20 were calculated using Eqs. 1, 2, and 3, respectively.

$$E = \frac{\sigma}{\varepsilon} = \left(\frac{P}{\Delta}\right)\frac{L}{A} \tag{1}$$

$$\nu_{12} = \frac{\varepsilon_2}{\varepsilon_1} \tag{2}$$

$$\text{UTS} = \frac{P_{\max}}{A} \tag{3}$$

where A area of cross-section of specimens, L span length, $\frac{P}{\Delta}$, slope of load–displacement curve under elastic range, $P_{\max}$ maximum load, ε_1 active strain parallel to the load, and ε_2 passive strain perpendicular to the load.

Shear modulus was calculated using Eq. 4 [24]. Since wood strands had a high slenderness ratio, the deformation was assumed to show no distortion. That is, St. Venant end effects can be ignored in the area away from the grips. For the evaluation of shear modulus (G_{LR}), E_1 for E_{L} and ν_{12} for ν_{LR} were obtained from the longitudinal-radial plane strands and E_2 for E_{R} was obtained from the radial-tangential plane strands, and the E_θ was obtained from the longitudinal-radial angled plane strands. For the evaluation of shear modulus (G_{LT}), E_1 for E_{L} and ν_{13} for ν_{LT} were

obtained from the longitudinal-tangential plane strands and E_3 for E_T was obtained from the tangential-radial plane strands, and the E_θ was obtained from the longitudinal-tangential angled plane strands. Shear strength was also measured from off-axis tension test using Eq. 5 [24]. τ_{LR} was obtained from the longitudinal-radial angled plane strands. τ_{LT} was obtained from the longitudinal-tangential angled plane strands.

$$G_{12} = \frac{1}{\left(-\frac{1}{E_1}\cos^4\theta - \frac{1}{E_2}\sin^4\theta + \frac{1}{E_\theta}\right)\frac{1}{\sin^2\theta\cos^2\theta} + \frac{2\upsilon_{12}}{E_1}} \quad (4)$$

$$\tau_{12} = \sigma_{max}\sin\theta\cos\theta \quad (5)$$

where θ, angle between global axis and grain direction for angled strands, E_1, elastic modulus from longitudinal-radial plane strands, E_2 elastic modulus from radial-tangential plane strands or from tangential-radial plane strands, υ_{12}, Poisson's ratio from longitudinal-radial plane strands or from longitudinal-tangential plane strands, and σ_{max} maximum tensile stress from longitudinal-radial angled strands or from longitudinal-tangential angled strands.

Orthotropic properties of loblolly pine strands

After all elastic properties and strength values from the different plane strands were determined, the orthotropic constitutive relationship for loblolly pine strands was constructed. Orthotropic constitutive equation is defined as

$$\begin{Bmatrix} \varepsilon_L \\ \varepsilon_R \\ \varepsilon_T \\ \gamma_{RT} \\ \gamma_{LT} \\ \gamma_{LR} \end{Bmatrix} = \begin{vmatrix} 1/E_L & -\upsilon_{RL}/E_R & -\upsilon_{TL}/E_T & 0 & 0 & 0 \\ -\upsilon_{LR}/E_L & 1/E_R & -\upsilon_{TR}/E_T & 0 & 0 & 0 \\ -\upsilon_{LT}/E_L & -\upsilon_{RT}/E_R & 1/E_T & 0 & 0 & 0 \\ 0 & 0 & 0 & 1/G_{RT} & 0 & 0 \\ 0 & 0 & 0 & 0 & 1/G_{LT} & 0 \\ 0 & 0 & 0 & 0 & 0 & 1/G_{LR} \end{vmatrix} \begin{Bmatrix} \sigma_L \\ \sigma_R \\ \sigma_T \\ \tau_{RT} \\ \tau_{LT} \\ \tau_{LR} \end{Bmatrix} \quad (6)$$

The orthotropic constitutive equation can be shortened as Eq. 7.

$$\{\varepsilon\} = [S]\{\sigma\} \quad (7)$$

The compliance matrix $[S]$ is symmetric that shows the following reciprocal relationship. Unknown Poisson's ratios from this study were obtained using the Eq. 8.

$$\frac{\upsilon_{TR}}{E_T} = \frac{\upsilon_{RT}}{E_R}, \quad \frac{\upsilon_{TL}}{E_T} = \frac{\upsilon_{LT}}{E_L}, \quad \frac{\upsilon_{RL}}{E_R} = \frac{\upsilon_{LR}}{E_L}, \quad (8)$$

The maximum strain values for loblolly pine strands from growth ring numbers 1–10 and 11–20 were calculated based on the relationship between strength values and compliance matrices. This was a reasonable calculation since an identical point between proportional limit and yield point was observed regardless of the orientation of wood strands. However, different oriented strands showed different failure modes due to the different strain distributions [25].

Failure modes

Figure 4 shows the different failure modes observed under tension loading. These failure modes were adapted from ASTM D 143 [26] testing of compression specimens. Shear failure describes failure occurring near 45° to the loading direction. Split failure describes failure similar to tearing in the middle with no distinctive angle. Wedge failure describes failure showing crack propagation along the grain. Shear along orientation failure describes crack propagation along the grain direction. Shear against orientation failure mode describes crack propagation across the grain direction.

Moisture content and specific gravity measurement

Moisture content and specific gravity were measured according to Method A of ASTM D 4442 [27] and Method A of ASTM D 2395 [28], respectively. Samples for both testing methods were obtained from the same populations using untested strands. To minimize the influence of the room humidity and temperature, all samples were kept in re-closable bags and handled by forceps when the specimens were mounted on the balance. The balance had a sensitivity of ±0.00001 g.

Results and discussion

Physical and mechanical test results

Table 2 shows the moisture content (MC) and specific gravity (SG) of loblolly pine strands from growth ring numbers 1–10 and 11–20. MC for the 10 groups showed low variability independent of cutting directions and growth ring numbers. SG increased as the growth ring number increased with the lowest SG of 0.33 occurred in LR 1–10 with coefficient of variation (COV) of 11.6%

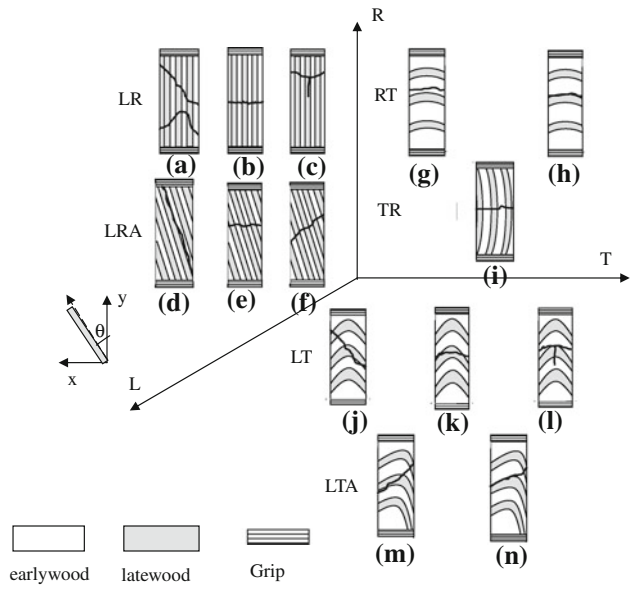

Fig. 4 Different failure modes under tension loading. **a** shear, **b** split, **c** wedge from the longitudinal-radial plane strands (LR), **d** shear along grain, **e** split, **f** shear against grain from the longitudinal-radial angled plane strands (LRA), **g** tear in earlywood, **h** tear in the boundary from the radial-tangential plane strands, **i** split from the tangential-radial plane strands, **j** shear, **k** split, **l** wedge from the longitudinal-tangential plane strands (LT), **m** shear, and **n** shear along grain from the longitudinal-tangential angled plane strands (LTA)

while the highest SG of 0.44 was found in LRA 11–20 with COV of 7.2%. The average SG and variation of SG were dependent upon growth ring numbers and cutting directions in this arrangement.

Table 3 shows the mechanical properties of strands from growth ring numbers 1–10 and 11–20. Since LRA 1–10 and LRA 11–20 had different orientation angles, no direct comparison between these two groups was made. The highest elastic modulus (E_L) of 2.75 GPa was obtained from LR 11–20 with COV of 14.1% while the lowest elastic modulus (E_T) of 0.39 GPa was obtained from TR 11–20 with COV of 58.3%, indicating that the elastic modulus was more related with orientation than specific gravity. A previous study also showed a poor correlation between specific gravity and elastic modulus [29]. It can be speculated that elastic modulus of the strands from different growth ring numbers was determined by earlywood and latewood fiber orientation associated with their ultrastructures including microfibril angle, cell wall thickness, and cell arrangement [7, 30]. Considering the trends of microfibril angle and cell wall thickness with growth ring position from the previous study [7, 8, 10], elastic modulus values from the LR and LT plane strands with increment of growth ring numbers were influenced by microfibril angle and cell wall thickness, whereas elastic modulus values with increment of growth ring numbers from the RT and TR plane strands were influenced by ray cells and cell arrangement in the radial and tangential direction [31, 32].

Regardless of growth ring number and orientation, the variation of Poisson's ratio was higher than the elastic modulus and UTS. In general, as growth ring number increased, the variation of Poisson's ratio decreased. The lowest Poisson's ratio (v_{TR}) of 0.21 was obtained from TR 11–20 with COV of 67.8% while the highest Poisson's ratio (v_{LT}) of 1.31 was obtained from LT 11–20 with COV of 42.7%. At the same growth ring number, v_{LR} from LR 1–10 was 43% lower than v_{LT} from LT 1–10 and v_{LR} from LR 11–20 had 118% lower than v_{LT} from LT 11–20. It can be speculated that the loblolly pine strands have a higher resistance to the radial direction than to the tangential direction. This could be the fact that ray cells may reinforce the radial direction [31–34]. This was also seen in the Poisson's ratio (v_{RT}), 1.07 for RT 1–10 and 1.1 for RT 11–20. Previous researchers pointed out the limit of Poisson's ratio for orthotropic material without violating elasticity theory [35–37]. From the limit equation for Poisson's ratio represented in the previous paper, the limit of v_{LT} and v_{RT} from growth ring numbers 11–20 could be 2.54 and 1.51, respectively, which indicated that the Poisson's ratio observed from this study can be verified. However, a comprehensive investigation on strain distribution related to ultrastructure arrangement associated with earlywood and latewood fiber orientation in wood strands is required for better understanding of the difference in Poisson's ratio values from different plane strands.

Shear modulus increased as the growth ring number increased, whereas shear strength decreased as the growth

Table 2 Physical properties of loblolly pine strands

Growth ring number 1–10	MC (%) (COV)	SG (COV)	Growth ring number 11–20	MC (%) (COV)	SG (COV)
LR 1–10	7.37% (4.2%)	0.33 (11.6%)	LR 11–20	7.69% (2.8%)	0.41 (5.0%)
LRA 1–10	6.97% (1.7%)	0.41 (8.1%)	LRA 11–20	6.74% (3.4%)	0.44 (7.2%)
LT 1–10	7.49% (2.3%)	0.37 (7.9%)	LT 11–20	7.41% (1.9%)	0.43 (14.7%)
LTA 1–10	N/A	N/A	LTA 11–20	6.54% (5.2%)	0.43 (8.4%)
RT 1–10	6.47% (7.7%)	0.39 (11.1%)	RT 11–20	6.50% (6.6%)	0.43 (15.1%)
TR 1–10	N/A	N/A	TR 11–20	6.78% (3.2%)	0.42 (7.6%)

Table 3 Summary of mechanical properties of loblolly pine strands from growth ring numbers 1–10 and growth ring numbers 11–20

Growth ring numbers 1–10	LR 1–10			LRA 1–10[a]			RT 1–10			G_{LR}[c] (GPa)	τ_{LR} (MPa)
	E_L (GPa)	σ_L (MPa)	ν_{LR}	E_θ (GPa)	σ_θ (MPa)	ν_θ	E_R (GPa)	σ_R (MPa)	ν_{RT}		
AVE	2.41	20.5	0.66	1.97	13.58	1.04	0.89	2.94	1.07	0.89	4.67
COV (%)	27.4	36.9	77.0	27.2	23.7	45.1	44.5	42.1	70.8		27.2
Growth ring numbers 11–20	LR 11–20			LRA 11–20[b]			RT 11–20			G_{LR}[c] (GPa)	τ_{LR} (MPa)
	E_L (GPa)	σ_L (MPa)	ν_{LR}	E_θ (GPa)	σ_θ (MPa)	ν_θ	E_R (GPa)	σ_R (MPa)	ν_{RT}		
AVE	2.75	29.0	0.60	2.46	16.96	0.72	0.88	2.52	1.1	1.11	4.09
COV (%)	14.1	23.6	35.6	22.9	18.8	36.5	44.7	33.1	56.7		26.2
Growth ring numbers 1–10	LT 1–10			LTA 1–10[d]			TR 1–10			G_{LT}[c] (GPa)	τ_{LT} (MPa)
	E_L (GPa)	σ_L (MPa)	ν_{LT}	E_θ (GPa)	σ_θ (MPa)	ν_θ	E_T (GPa)	σ_T (MPa)	ν_{TR}		
AVE	2.47	20.5	0.95	N/A	N/A	N/A	N/A	N/A	N/A	N/A	N/A
COV (%)	22.9	24.6	41.6	N/A	N/A	N/A	N/A	N/A	N/A	N/A	N/A
Growth ring numbers 11–20	LT 11–20			LTA 11–20[e]			TR 11–20[e]			G_{LT}[c] (GPa)	τ_{LT} (MPa)
	E_L (GPa)	σ_L (MPa)	ν_{LT}	E_θ (GPa)	σ_θ (MPa)	ν_θ	E_T (GPa)	σ_T (MPa)	ν_{TR}		
AVE	2.53	23.5	1.31	1.98	4.35	0.29	0.39	1.11	0.21	0.593	2.01
COV (%)	31.7	31.1	42.7	76.4	49.2	72.1	58.3	34.1	67.8		34

[a] LRA 1–10 has the average grain angle of 33.4 degree with a COV of 16.7%

[b] LRA 11–20 has the average grain angle of 23.5 degree with a COV of 16.0%

[c] Calculated values of shear modulus based on average test values using Eq. 4

[d] LTA 1–10 has the average grain angle of 30 degree

[e] LTA 11–20 has the average grain angle of 30 degree

ring number increased. The shear strength may be more dependent upon the structure of earlywood and latewood bands. The ratio of latewood MOE to earlywood MOE increased as the growth ring number increased [9]. The higher ratio of latewood to earlywood MOE could cause stress concentrations between the growth ring boundaries resulting in a lower shear strength value. Shear modulus, however, was measured using the average elastic properties of wood strands, which were smeared properties from elastic properties of earlywood and latewood bands.

The highest UTS of 29.0 MPa was obtained from LR 11–20 with COV of 23.6% while the lowest UTS of 1.11 MPa was obtained from TR 11–20 with COV of 34.1%, which followed similar trends with elastic modulus. In general, as growth ring number increased, UTS increased, except for the RT plane strands showing slight decrements. Different UTS values from different plane strands indicated that orientation of earlywood and latewood band associated with earlywood and latewood fiber direction to the loading appeared to be a key variable in determination of UTS.

The UTS values from LR 1–10 and LT 1–10 were similar while UTS from LR 11–20 was higher than LT 11–20. Higher microfibril angle and thinner cell wall thickness of earlywood and latewood from growth ring numbers 1–10 may lead to similar UTS values between LR 1–10 and LT 1–10 [8–10]. Compared to the growth ring numbers 1–10, lower microfibril angle and thicker cell wall thickness reinforced earlywood and latewood fibers, which might lead to more distinctive different stress distribution within the LR and LT plane strands and resulted in different UTS values [38].

Statistical comparisons

Table 4 shows the statistical results from comparisons of the elastic modulus, UTS, and Poisson's ratio values for different growth ring numbers and strand orientations. An alpha value of 0.05 was used for all ANOVA tests. Strands from different growth ring numbers showed that only the LR plane strands were significantly different for elastic modulus and UTS. It can be interpreted that elastic modulus and UTS from the LR plane strands were controlled by earlywood and latewood cell properties including cell wall thickness and microfibril angle. However, elastic modulus and UTS from the LT and RT plane strands were controlled by earlywood and latewood band arrangement associated with earlywood and latewood cell arrangement.

Table 4 Statistical comparisons of elastic modulus, UTS, and Poisson's ratio for loblolly pine strands from the different growth ring numbers and planes

Growth ring numbers effect	Elastic modulus *p*-value	UTS *p*-value	Poisson's ratio *p*-value
LR 1–10 vs. LR 11–20	0.01	<.0001	1.00
LT 1–10 vs. LT 11–20	0.75	0.57	0.40
RT 1–10 vs. RT 11–20	0.77	1.0	0.83
Orientation effect	Elastic modulus *p*-value	UTS *p*-value	Poisson's ratio *p*-value
LR 1–10 vs. LT 1–10	0.69	1.0	0.31
LR 11–20 vs. LT 11–20	0.15	<.0001	<.0001
LR 1–10 vs. LRA 1–10	0.017	<.0001	0.07
LR 11–20 vs. LRA 11–20	0.007	<.0001	0.97
LT 11–20 vs. LTA 11–20	<.0001	<.0001	<.0001
RT 11–20 vs. TR 11–20	<.0001	<.0001	<.0001

At growth ring numbers 1–10, elastic modulus and UTS between the LR and LT plane strands were not significantly different, respectively. It can be speculated that earlywood and latewood cells from growth ring numbers 1–10 were not distinctively different in the radial and tangential direction associated with earlywood and latewood bands arrangement. It may also be the reason for showing no significant difference in the Poisson's ratio between LR 1–10 and LT 1–10.

At growth ring numbers 11–20, elastic modulus between the LR and LT plane strands was not significantly different but the UTS between the LR and LT plane strands was significantly different. Longitudinal elastic modulus (E_L) was highly dependent upon the longitudinal properties of earlywood and latewood fibers [9, 25]. Since earlywood and latewood fibers were aligned in the longitudinal direction for the LR and LT plane strands, the longitudinal elastic modulus between LR 11–20 and LT 11–20 was not significantly different. However, UTS was highly related to the stress distribution [38]. Earlywood and latewood band-associated earlywood and latewood fiber properties created different stress distribution in LR 11–20 and LT 11–20, which may result in significant differences in UTS and Poisson's ratio between two different plane strands.

The statistical comparison of Poisson's ratio for the 10 groups indicated that there was not a significant difference between the different growth ring numbers while there was a significant difference between the different orientations. This is not surprising because Poisson's ratio was calculated from two different strains that were highly dependent upon the geometry of strands. However, it should be noted that the COV of Poisson's ratio ranged from 77 to 35%, which indicated that the statistical comparisons for Poisson's ratio provided in this study were limited.

Orthotropic properties of loblolly pine strands

Figure 5 shows the orthotropic properties for loblolly pine strands from growth ring numbers 1–10 and 11–20. With increment of growth ring numbers from 1–10 to 11–20, the ratio of E_L to E_R increased from 2.71 to 3.12 but the ratio of E_L to G_{LR} decreased from 2.71 to 2.48. The ratio of E_L to E_T from the growth ring numbers 11–20 was the highest 7.05, followed by the ratio of E_L to G_{LT} 4.64. The elastic modulus ratios of E_R to E_T and G_{LR} to G_{LT} indicated that elastic properties in the tangential directions were much weaker than the radial direction. Different elastic modulus ratios indicated that elastic behavior of wood strands was highly dependent upon the loading direction to the orientation of earlywood and latewood fibers (Fig. 5a).

The strength ratio showed similar trends compared to the elastic modulus ratio, but it showed much more distinctive differences (Fig. 5b). The longitudinal strength (σ_L) of loblolly pine strands from growth ring numbers 11–20 was noticeably higher than that of strands from growth ring numbers 1–10. With increment of growth ring numbers from 1–10 to 11–20, the ratio of σ_L to σ_R increased from 6.97 to 11.51 and the ratio of σ_L to τ_{LR} increased from 4.39 to 7.09. The ratio of σ_L to σ_T from growth ring numbers 11–20 was the highest 26.13, followed by the ratio of σ_L to τ_{LT} 14.42. The strength ratios of σ_R to σ_T and τ_{LR} to τ_{LT} indicated that strength of loblolly pine strands in the tangential direction was much weaker than the radial direction. Different strength ratios indicated that the longitudinal fiber direction was the strongest direction from loblolly pine strands, whereas the tangential fiber direction was the weakest direction.

Normal strains (ε_L, ε_R, ε_T) and shear strains (γ_{LR}, γ_{LT}, γ_{RT}) of loblolly pine strands from growth ring numbers 1–10 and 11–20 were calculated using Eqs. 6 and 7. For growth ring numbers 1–10, elastic modulus (E_T) was

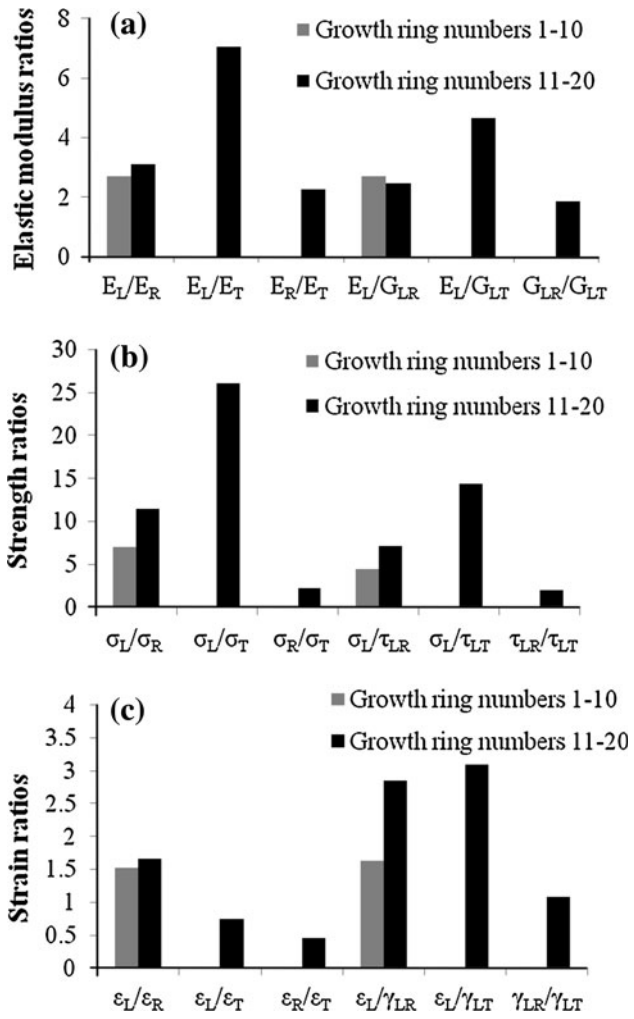

Fig. 5 Orthotropy ratios of loblolly pine strands from growth ring numbers 1–10 and 11–20. **a** Elastic ratios of loblolly pine strands from growth ring numbers 1–10 and 11–20. **b** Strength ratios of loblolly pine strands from growth ring numbers 1–10 and 11–20. **c** Strain ratios of loblolly pine strands from growth ring numbers 1–10 and 11–20

assumed to be equivalent to E_R. Shear modulus (G_{LT} and G_{RT}) was assumed to be equivalent to G_{LR}, and shear strength (τ_{LT}, τ_{RT}) was assumed to be equivalent to τ_{LR}. For growth ring numbers 11–20, shear modulus (G_{RT}) was assumed to be equivalent to G_{LT}, and shear strength (τ_{RT}) was assumed to be equivalent to τ_{LT}. These assumptions were reasonable because elastic modulus and strength in the tangential direction was much lower than the longitudinal and radial direction (Table 3). However, only calculated strain values from experimentally determined elastic properties and strength values were presented in Fig. 5c.

Compared to growth ring numbers 1–10, the strain ratios of ε_L to ε_R and ε_L to γ_{LR} of loblolly pine strands from growth ring numbers 11–20 were higher, respectively, indicating that a larger longitudinal deformation and smaller shear deformation could be observed in loblolly pine strands from growth ring numbers 11–20 (Fig. 5c). The strain ratios from growth ring numbers 11–20 indicated that maximum allowable deformation in the normal directions (L, R, and T) was higher than the shear deformations. Different magnitudes of normal and shear strains of loblolly pine strands were also observed from differently oriented strands from Jeong [39], and Jeong and Hindman [25].

Although loblolly pine strands showed orthotropic behavior regardless of growth ring numbers, higher orthotropic property ratios were observed from a higher growth ring number. The different maximum stress and strain values for loblolly pine strands from the two different growth ring numbers led to different failure behavior associated with different orientations of earlywood and latewood bands in strands.

Failure modes

Failure behavior of the 10 different wood strand groups was distinctively different (Table 5). While LR 1–10

Table 5 Failure behavior of different orientation loblolly pine strands

Sample	Shear (%)	Split (%)	Wedge (%)	Shear along grain (%)	Shear against grain (%)	Tear within earlywood	Tear between earlywood and latewood
LR 1–10	30.0	30.0	40.0	0	0	0	0
LR 11–20	70.0	26.7	3.3	0	0	0	0
LRA 1–10	0	46.8	0	34.3	18.7	0	0
LRA 11–20	0	6.45	0	93.5	0	0	0
LT 1–10	56.2	40.6	3.1	0	0	0	0
LT 11–20	37.5	53.1	9.4	0	0	0	0
LTA 11–20	6.45	0	0	93.5	0	0	0
RT 1–10	0	0	0	0	0	66.6	33.3
RT 11–20	0	0	0	0	0	16.6	83.3
TR 11–20	0	100	0	0	0	0	0

showed no dominant failure mode, LR 11–20 showed mostly shear failures. Interestingly, LRA 1–10 showed 18.75% shear against the orientation failures, indicating that the earlywood and latewood band orientation was not the dominant factor controlling the crack propagation, whereas LRA 11–20 showed dominantly shear along the orientation failures with no shear against orientation failure modes. The LR and LRA plane strands from growth ring numbers 11–20 showed more uniform failure types that could infer more directional reinforcement in the longitudinal direction. The directional reinforcement at the cellular level was observed from the previous studies showing that with increment of growth ring number, the average value of microfibril angle decreased and cell wall thickness increased [7, 8, 10, 40].

LT 1–10 and LT 11–20 showed failures susceptible to the orientation of earlywood and latewood. LTA 11–20 showed shear along the orientation failures dominantly similar to the LRA 11–20. These particular different types of failure for differently oriented wood strands were highly associated with different stress distributions that originated from different orientation of earlywood and latewood bands, and this is important to predict the UTS [38].

The RT plane strands had either tear failures occurred in the earlywood bands or failures occurred in the boundary between earlywood and latewood bands. RT 1–10 had 66.6% tear failures within earlywood bands followed by 33.3% failures in the boundary between earlywood and latewood bands. RT 11–20 showed 83.3% of failures in boundary between earlywood and latewood bands with only 16.7% tear failures in earlywood bands. Lower elastic modulus ratio of latewood to earlywood from growth ring numbers 1–10 created smooth stress transitions between earlywood and latewood bands, which created failures in mostly earlywood bands where the least stiffness and greater variation existed [9, 40]. As growth ring number increased, narrower earlywood bands and higher ratio of latewood to earlywood elastic modulus created an abrupt stress distribution between earlywood and latewood and led to failures in the boundary between earlywood and latewood [9, 38]. TR 11–20 showed split failures dominantly and some shear along the orientation failures. Based on strain ratios from Fig. 5, maximum tangential strain was much higher than maximum radial strain at the same loading level, which may result in split failures along the radial direction.

Previous studies showed similar failure behavior in the RT and TR plane observed at the cellular level [41–43]. When the TR plane specimen was loaded in the tangential direction, crack propagated in the radial direction through cell separation resulting in minor deviations and smooth crack surfaces. For the RT plane specimen, cracks propagated within the earlywood band parallel to the annual ring and perpendicular to the loading direction through rupturing the cell walls, leading to rough surfaces. Conrad et al. [44] reported that cell fracture had higher fracture toughness than cell separation. This was shown by a higher UTS of the RT plane strands over the TR plane strands (Table 3).

The distinctive difference in mechanical properties from wood strands between growth ring numbers 1–10 and 11–20 indicated that the ratio of orthotropic properties increased with increment of growth ring numbers. Orientation of earlywood and latewood to the loading direction and the ratio of elastic properties produced different stress and strain distributions [39] and led to the different failure modes. More consistent failure behavior of strands from growth ring numbers 11–20 can be associated with more distinctive differences in orthotropic properties compared to the growth ring numbers 1–10 (Fig. 5). Based on the results, more mature wood (growth ring number 11–20) had more directional reinforcement while more juvenile wood (growth ring number 1–10) had more variation on the orientation of its structure.

Conclusions

Mechanical properties of loblolly pine strands from growth ring numbers 1–10 and 11–20 were examined using tension tests incorporating DIC. Loblolly pine strands showed orthotropic elastic behavior associated with distinctive failure modes. Elastic modulus, Poisson's ratio, shear modulus, shear strength, and UTS from loblolly pine strands were more dependent upon the earlywood and latewood orientation compared to specific gravity. In general, the elastic modulus and UTS increased as growth ring number increased. However, Poisson's ratio was not dependent upon growth ring positions but the orientation. With increment of growth ring number, shear modulus increased but shear strength decreased.

Comparing elastic modulus and strength values from the two different growth ring positions, a significant increase occurred in the longitudinal elastic modulus and strength from growth ring numbers 11–20, which indicated that wood structure may develop to reinforce the longitudinal direction.

Maximum strain values from loblolly pine strands were distinctively different between growth ring numbers 1–10 and 11–20. Compared to loblolly pine strands from growth ring numbers 1–10, loblolly pine strands from growth ring numbers 11–20 had higher maximum normal strains and lower maximum shear strains. These orthotropic behaviors associated with growth ring positions were highly related to failure modes. Although strands showed mixed failure modes, strands from growth ring numbers 11–20 showed

more consistent failure mode, indicating that directional reinforcement and less variability of structure were developed in higher growth ring position strands.

Evaluated orthotropic properties associated with failure behaviors can be used as input properties and intuitive modeling assumptions for wood strands and strand-based composites.

Acknowledgements This study was funded by the USDA National Research Initiative Competitive Grants Program (2005-35504-16115). Their financial contribution to this study is greatly appreciated.

References

1. Bodig J, Goodman JR (1973) Wood Sci 5:249
2. Gunnerson RA, Goodman JR, Bodig J (1972) Wood Sci 5:241
3. Hermon RFS (1961) An introduction to applied anisotropic elasticity. Oxford University Press, London, England
4. Cai Z, Wu Q, Han G, Lee JN (2007) Forest Prod J 57:36
5. Hindman DP, Lee JN (2007) Wood Fiber Sci J 39:515
6. Jeong GY, Hindman DP, Finkenbinder D, Lee JN, Lin Z (2008) Forest Prod J 58:33
7. Cramer SM, Kretschmann DE, Lakes R, Schmidt T (2005) Holzforschung 59:531
8. Groom L, Mott L, Shaler S (2002) Wood Fiber Sci J 34:14
9. Jeong GY, Zink-Sharp A, Hindman DP (2009) Wood Fiber Sci J 41:51
10. Larson PR, Kretschmann DE, Clark III A, Isebrands JG (2001) Juvenile wood formation and properties in southern pine. General technical report FPL-GTR-129. USDA, Forest Service, Forest Products Laboratory, Madison, Wisconsin
11. Clouston P (2007) Holzforschung 61:394
12. Clouston P, Lam F (2002) Compos Sci Technol 62:1381
13. Wang YT, Lam F (1998) Comp Mater Sci 11:157
14. Deomano EC, Zink-Sharp A (2005) Forest Prod J 55:31
15. Geimer RL, Mahoney RJ, Loehnertz SP, Meyer RW (1985) Forest Prod J 50:33
16. Price EW (1975) Forest Prod J 26:50
17. Wu Q, Cai Z, Lee JN (2005) Forest Prod J 52:1
18. Zhang W, Sliker A (1991) Wood Fiber Sci J 21:58
19. Galicki J, Czech M (2005) Mech Mater 37:677
20. Bergander A, Salmen L (2002) J Mater Sci 37:151. doi:10.1023/A:1013115925679
21. Mott L, Shaler SM, Groom LH (1996) Wood Fiber Sci J 28:429
22. Baxter SC, Graham LL (2000) ASCE J Eng Mech 126:389
23. Baxter SC, Hossain MI, Graham LL (2001) Int J Solids Struct 38:9209
24. Jones RM (1975) Mechanics of composite materials. McGraw-Hill, New York, p 55
25. Jeong GY, Hindman DP (2010) Wood Fiber Sci J 42:51
26. American Society for Testing and Materials (ASTM) (2005a) ASTM D 143. Standard test methods for small clear specimens of timber. In: Annual book of ASTM standard, sect 4, vol 04.10 Wood. ASTM, West Conshohocken, PA
27. American Society for Testing and Materials (ASTM) (2005b) ASTM D 4442. Standard test methods for direct moisture content measurement of wood and wood-base materials In: Annual book of ASTM standard, sect 4, vol 04.10 Wood. ASTM, West Conshohocken, PA
28. American Society for Testing and Materials (ASTM) (2005c) ASTM D 2395. Standard test methods for specific gravity of wood and wood-based materials. In: Annual book of ASTM standard, sect 4, vol 04.10 Wood. ASTM, West Conshohocken, PA
29. Zhang SY (1997) Wood Sci Technol 31:181
30. Salmen L, Burgert I (2009) Holzforschung 63:121
31. Bergander A, Salmen L (2000) Holzforschung 54:654
32. Reiterer A, Burgert I, Sinn G, Tschegg S (2002) J Mater Sci 37:935. doi:10.1023/A:1014339612423
33. Beery WH, Ifju G, McLain TE (1983) Wood Fiber Sci J 15:395
34. Saka S, Thomas RJ (1982) Wood Sci Technol 16:167
35. Janowiak JJ, Hindman DP, Manbeck HB (2001) Wood Fiber Sci J 33:580
36. Lempriere BM (1968) AIAA J 6:2226
37. Theocaris PS (1994) J Mater Sci 29:3527. doi:10.1007/BF00352058
38. Jeong GY, Hindman DP (2009) J Mater Sci 44:3824. doi:10.1007/s10853-009-3518-4
39. Jeong GY (2008) Tensile properties of loblolly pine strands using digital image correlation and stochastic finite element method. Ph.D thesis, Blacksburg, Virginia Tech
40. Anagnost SE, Mark RE, Hanna RB (2005) IAWA J 26:325
41. Gibson LJ, Ashby MF (1998) Cellular solids, structure and properties. Pergamon Press, Oxford
42. Jernkvist LO, Thuvander F (2001) Holzforschung 55:309
43. Wittel FK, Dill-Langer G, Kroplin BH (2005) Comp Mater Sci 32:594
44. Conrad MPC, Smith GD, Fernlund G (2003) Wood Fiber Sci J 35:570